Full length article

FBG bandwidth impact on dual-comb interrogation for high fidelity strain sensing

Malhar A. Nagar [a,*], Minghao Wei [b,c], Alejandro Rosado [b,c], Conor McArdle [b], Aleksandra Kaszubowska-Anandarajah [c], Prince M. Anandarajah [b,c], Davide Janner [a,*]

[a] Dipartimento di Scienza Applicata e Tecnologia (DISAT), Politecnico di Torino, Corso Duca degli Abruzzi, 24, 10125 Turin, Italy
[b] Photonics Systems and Sensing Lab (PSSL), School of Electronic Engineering, Dublin City University, Glasnevin, Dublin 9, Ireland
[c] CONNECT Research Centre, Electronic and Electrical Engineering, School of Engineering, Trinity College Dublin, D02 W272, Ireland

ABSTRACT

Dual Optical Frequency Comb (DOFC) interrogation has emerged as a promising approach for high-resolution Fiber Bragg Grating (FBG) sensing, yet its robustness across gratings of differing spectral bandwidths remains insufficiently explored. Two key gaps persist: first, the lack of systematic evaluation of a single DOFC platform applied consistently to both narrow- and broadband FBGs; and second, the absence of a unified signal-processing strategy that maintains accuracy under variable spectral sampling conditions. Here, we address these challenges by developing a bandwidth-adaptive DOFC interrogation framework that unifies optical and algorithmic optimization across diverse FBG bandwidths. To the best of our knowledge, this is the first systematic assessment of a mutually coherent dual-comb system applied to multiple FBG bandwidth regimes within a single interrogation platform. The system employs Externally-Injected Gain-Switched Lasers (EI-GSLs) to generate two mutually coherent combs and a custom ADC-FFT module enabling real-time spectral acquisition. A spectral-envelope-assisted inverted Gaussian fitting (IGF) algorithm is implemented to reconstruct sparsely sampled FBG notches and extract precise Bragg wavelength shifts. Experiments on FBGs with 0.1 nm and 0.3 nm bandwidths demonstrate consistent high-fidelity strain tracking, achieving effective detection limits of $\sim$ 375–380 nε, dynamic ranges up to 1300 $\mu\varepsilon$, and linearity of $R^2 \approx 0.98$. Compared with a state-of-the-art swept-laser interrogator, which fails to resolve at the finest nano-strain increments, the proposed DOFC-IGF approach delivers superior stability and resolution across all tested bandwidths. These findings establish a practical framework for bandwidth-adaptive DOFC interrogation, enabling scalable and cost-effective deployment of mixed-bandwidth FBG arrays in high-resolution sensing networks.

1. Introduction

High-resolution static strain sensing plays a pivotal role in applications ranging from aerospace structural health monitoring to biomedical instrumentation and precision metrology [1,2,3]. Fiber Bragg Gratings (FBGs) have emerged as a leading platform for these tasks, owing to their inherent strain sensitivity ($\sim$1 pm/$\mu\varepsilon$), spatial resolution, multiplexing capability, and compatibility with optical fiber networks [2]. The ability to interrogate FBGs with sub-microstrain resolution is therefore of fundamental and practical interest [4]. Conventional FBG interrogation techniques can be broadly divided into wavelength/frequency-domain and intensity/time-domain approaches. Wavelength-based methods, including the use of broadband ASE sources – optical spectral analyzers,

tunable laser scans – photodetector array, and integrated devices such as an arrayed waveguide grating (AWG), offer direct spectral reconstruction. However, these methods often suffer from limited refresh rates, bulky hardware, or high cost, limiting their deployment for commercial/industrial applications. Intensity-based schemes, such as edge-filter detection, tunable Fabry-Pérot filters, or slope-detection methods, provide compact and low-cost alternatives, but are typically constrained in resolution, linearity and multiplexing capability. As a result, these methods face several trade-offs among spectral resolution, speed, scalability, and robustness [5,6], potentially compromising their use for multiple and diverse strain-sensitive applications. In contrast, dual-comb spectroscopy (DCS) measures the spectral response of a sample using two mutually coherent optical frequency combs (OFCs) with

---

slightly different free spectral ranges (FSRs). Once these two OFCs are combined and photodetected, the optical features of the combined signal are down-converted into the radio-frequency (RF) domain, enabling a quick, absolute-frequency referenced readout without mechanical scanning [7,8]. A key enabler for compact, low-cost DCS is the use of gain-switched semiconductor lasers, which are subjected to optical injection (OI) [9]. The use of OI provides a stable phase reference to the dual comb system, making both combs coherent while improving their performance in terms of wavelength stability, carrier-to-noise ratio, and spectral bandwidth [10]. Such Externally-Injected Gain-Switched Laser (EI-GSL) sources have demonstrated coherent dual-comb operation with extremely high amplitude stability of individual lines (<0.3 dB), and practical spectroscopy performance in using cost-effective, simple and robust hardware [10,11] with a strong potential for integration.

The use of a DOFC for FBG interrogation allows the direct mapping of the FBG optical features into the RF spectra. Typically, one of the combs (or both) is (are) transmitted/reflected by the FBG, directly affecting its tone amplitude. The combined signal is subsequently photodetected, resulting in an RF comb envelope that now showcases the FBG features. Bragg wavelength shifts can then be tracked through changes in this RF comb envelope. Prior demonstrations using electro-optic [12], mode-locked fiber-laser [13,14], and gain-switched combs [15] have confirmed that DCS enables rapid and precise interrogation. A central challenge, however, lies in spectral sampling density. When the OFC's FSR is comparable to or larger than the 3 dB width of the FBG transfer function (i.e., FBG's transmission spectra in this case), it results in a few OFC tones sampling the FBG. Under such sparse-sampled conditions, the apparent spectral envelope and the accuracy of Bragg wavelength dip localization no longer reflect the complete intrinsic FBG transfer function directly, but rather depend on how the discretely sampled spectrum is reconstructed or interpolated during post-processing [4,16,17].

In this regime, the fidelity of demodulation relies strongly on digital signal processing strategies designed to recover the spectral peak from limited data points. Existing DCS interrogations can be broadly divided into two classes: (i) direct grid-based estimators such as weighted-centroid or barycentric tracking [18], fixed dB edge or half-power thresholding, and discrete cross-correlation [4]; and (ii) Parametric or model-based estimators, such as nonlinear least-squares fits [14,15], spline models, or multi-optimization template-matching [13]. While the first approach is computationally efficient and hardware-compatible, it is prone to comb spacing dependent bias and noise-driven variance under sparse or asymmetric sampling. Whereas the latter approach mitigates this bias by imposing known spectral shape constraints, though at greater computational cost and with sensitivity to model mismatch. Since the effective spectral resolution in dual-comb interrogation is ultimately determined by the comb spacing, the interpolation method and estimator choice significantly influence the localization error. Each approach carries bandwidth dependent trade-offs. For instance, narrow gratings (~0.1 nm) may be sampled by only a couple of comb lines, resulting in reduced fitting robustness, as small variations in individual optical tone amplitudes or phase noise can lead to significant uncertainty in estimating the central Bragg wavelength shift. Conversely, broader gratings provide a denser sampling grid but exhibit increased sensitivity to amplitude fluctuations and spectral baseline noise, as a larger portion of the comb interacts with weaker sidelobes or non-uniform FBG regions. This interplay underscores the need for adaptive interpolation and fitting pipelines that remain robust across varying bandwidths of FBGs when interrogated by a common DCS system. Thus, two gaps are particularly evident, firstly, the systematic evaluation of utilizing the same DOFC interrogation methodology across different FBG bandwidths. Secondly, most existing signal processing pipelines are optimized for FBGs with a specific spectral bandwidth, which limits their applicability when the same DCS interrogation system is used with gratings of different bandwidths. This raises a question of whether a unified strategy can be applied across both narrow and broad-

bandwidth gratings while maintaining accuracy and robustness. Addressing these gaps is essential for advancing DOFC from laboratory demonstrations toward real-world distributed sensor networks with mixed-bandwidth arrays. Indeed, previously [4], we demonstrated EI-GSL-based DOFC interrogation only on a single FBG with a 0.5 nm bandwidth using an electrical spectrum analyzer-based readout and non-adaptive demodulation, primarily focusing on various signal processing techniques to track FBG shifts.

To bridge these gaps and expand our previous work significantly for practical applications, this study systematically investigates the performance of EI-GSL based DOFC interrogation across FBGs of varying bandwidths, ~0.1, ~0.3, and ~0.5 nm, leveraging a custom built ADC-FFT module for real-time signal acquisition. To address how the FBG bandwidths affect the interrogation performance and the bandwidth related sampling challenges of gratings, we developed an inverted Gaussian fitting (IGF) pipeline that adapts to the number of comb lines overlapping each notch. This study thus extends dual-comb interrogation from single-bandwidth demonstrations to a framework applicable across mixed-bandwidth FBG arrays.

2. Experimental setup

The experimental configuration was designed to evaluate the static-strain sensing performance of FBG sensors with various bandwidths using EI-GSL based DOFC. The setup also allows systematic comparison of sensor metrics (e.g., sensitivity, linearity, and resolution) by benchmarking it against a state-of-the-art commercial FBG interrogator. The overall schematic is shown in Fig. 1.

The DOFC interrogation module was realized using two gain-switched semiconductor laser diodes. Two Fabry-Pérot lasers (Pilot Photonics – FP 203 and FP 204) were gain-switched with a combination of a bias current ($I_{bias1} = 22$ mA, $I_{bias2} = 15$ mA), provided by the current controller (Koheron CTL20-2), and two RF signals, generated by two synthesizers (ADF4356 BCPZ) and both amplified up to 23 dBm, with repetition rates of 1 GHz and 999.98 MHz, respectively, resulting in a repetition rate difference or frequency offset of (Δf) of 20 kHz. Additionally, external injection from a wavelength tunable semiconductor laser (Pure Photonics, PPCL700, 15 kHz) provides a stable wavelength reference and ensures mutual coherence between the two OFCs. To guarantee the gain switching of both secondary lasers is time synchronized, one synthesizer is set to function as the primary and the other as a secondary source via a 10 MHz reference clock. This is critical for the coherent heterodyning and down-converting of both combs to the RF domain. The DOFC interrogator was housed in a compact, thermally insulated enclosure to minimize effects from environmental changes. Subsequently, operational performance of the interrogator in terms of a 30-min amplitude stability test was carried out with the aid of a high-resolution optical spectrum analyzer (APEX AP2083A with a resolution of 0.16 pm). This test yielded results that showed reduced amplitude fluctuations of each OFC (below 0.3 dB across the 54 lines that lie within a 3 dB bandwidth). It is important to note that coarse wavelength tunability can be achieved by optically injecting into different FP modes, while fine wavelength tunability could be achieved by changing the bias current or temperature of the FP lasers [19]. In addition, the FSR of each comb can be changed by simply altering the frequency of the respective synthesizer used to modulate it. Hence, the wavelength and the FSR of the DOFC interrogator can be matched to the bandwidth of the FBG, thereby optimizing interrogation sensitivity and dynamic range. The comb outputs were combined via a 50:50 polarization-maintaining coupler and routed to a programmable optical band-pass filter (OBPF, WaveShaper 1000s). It was used to remove comb lines below the injection, including the injection wavelength, thus essentially isolating the unique RF beat tone frequencies overlapping the FBGs [10]. All fiber components inside the DOFC enclosure, including the coupler, utilize polarization-maintaining fiber to mitigate polarization induced instabilities arising from temperature, humidity and injection conditions.
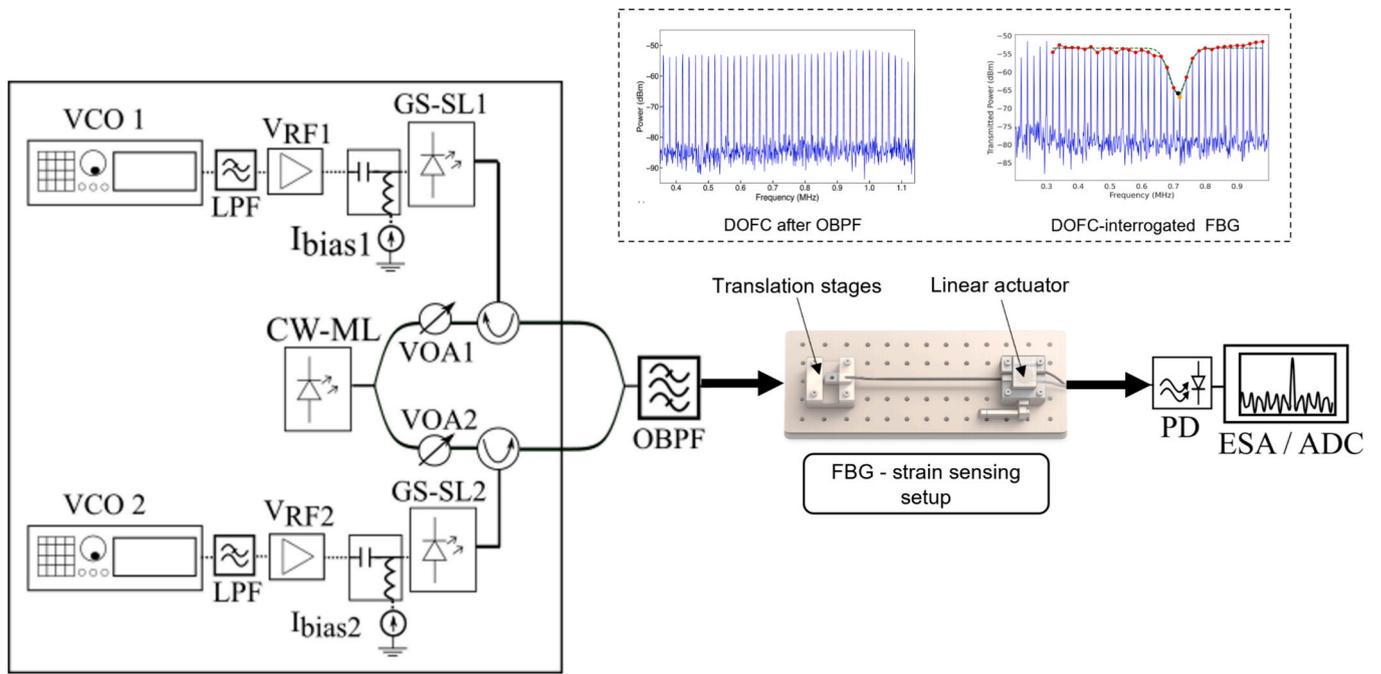
Fig. 1. Experimental setup for static strain sensing of FBGs using Externally-Injection Gain-Switched Lasers (EI-GSL) based Dual Optical Frequency Comb (DOFC) interrogation system. VCO – Voltage Controlled Oscillator, GS-SL – Gain Switched Slave Laser, CW-ML- Continuous Wave Master Laser, LPF – Low Pass Filter, V_{RF} – RF drive voltage, VOA- Variable Optical Attenuator, OBPF – Optical Band Pass Filter. The inset shows representative DOFC spectra after OBPF and after transmission through the FBG in RF domain.
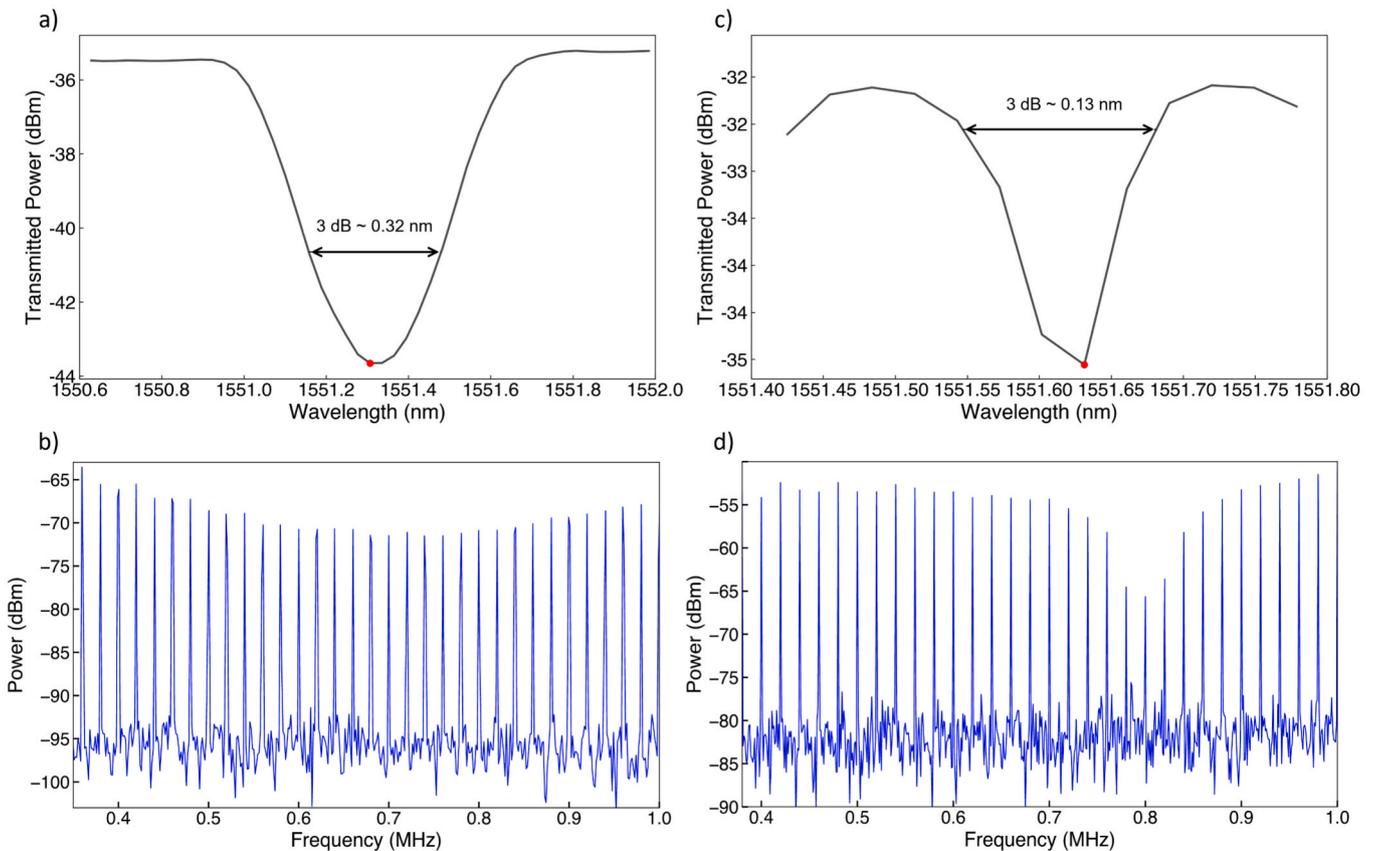

Fig. 2. Comparison of transmitted spectra for FBG1: (a) optical-domain transmission spectrum (in gray) and (b) corresponding RF-domain spectrum (in blue) after DOFC interrogation; and for FBG2: (c) optical-domain transmission spectrum and (d) corresponding RF-domain spectrum after DOFC interrogation.

The output of the OBPF was directed through the FBGs, and the transmitted signal was detected by a low-speed photodetector (Thorlabs PDA10CF). The photodetector output was subsequently digitized and processed using a custom prototype ADC-FFT module, which integrates a 14-bit ADC (ADC14L020) operating at 10 MSPS with a 600 MHz NXP iMXRT1062 ARM Cortex-M7 microcontroller, providing USB interfacing and on-board FFT capability for real-time spectral recording. For calibration, the FBGs were mounted on a precision translation stage (Thorlabs MAX313D/M − 3-Axis NanoMax Stage), with one end affixed to a linear piezoelectric actuator (PI-753 LISA), controlled via PZT-servo controller (PI E-501 modular piezo controller).

Two FBGs were employed as sensing elements, (i) FBG1 − centered at 1551.31 nm with a bandwidth of ∼ 0.32 nm, and (ii) FBG2 − centered at 1551.62 nm with a narrower bandwidth of ∼ 0.13 nm. Their complementary spectral responses enabled direct assessment of interrogation performance as a function of grating bandwidth. The corresponding transmission optical spectra of the FBGs are shown in Fig. 2a) and c), while Fig. 2b) and d) show the associated unique down-converted RF spectra after DOFC interrogation. Together, these plots illustrate the mapping of the FBG spectral features from the optical domain to the RF domain via dual-comb heterodyne detection. For clarity on the mutual spectral arrangement, Fig. S1 presents representative optical-domain spectra of the individual OFCs under injection locking, acquired using a high-resolution optical spectrum analyzer prior to optical band-pass filtering. The calibration process involved systematically applying known strain increments to the FBGs using the PZT and recording the corresponding spectral responses. Controlled strain increments in various step sizes were applied via the PZT by imposing calibrated displacements of 1 μm, 100 nm, 50 nm, and 10 nm, corresponding to strains of 3.33 με, 0.33 με, 0.17 με, and 33.3 nε, respectively. This configuration facilitated the systematic assessment of the system's sensitivity and linearity over a wide range of strain values.

To validate the performance of the DOFC interrogation system, the FBGs were also interrogated using a commercial Smart Scan interrogator (Smart Fibres), which serves as a benchmark due to its widespread use and established reliability. Calibration plots obtained from the DOFC-based methods were compared with those from the Smart Scan interrogator, which reconstructs the FBG reflection spectrum using a swept-laser source with dense spectral sampling and internal averaging, from which the Bragg wavelength is estimated using proprietary signal-processing routines. In this study, the system was operated under its recommended static-strain configuration setting, at a 2.5 Hz acquisition rate, with 1000 averaging and a single-file integration time of ∼ 4.5 s, to ensure optimal wavelength stability and a fair comparison. Additionally, FBGs were kept under enclosed environment to minimize air-flow driven fluctuations and short-term thermal transients.

3. Methodology

Accurate determination of Bragg wavelength shifts from the DOFC-interrogated FBG spectra requires robust signal processing capable of extracting sub-picometer wavelength shifts from the down-converted RF comb data. Mutual coherence between the EI-GSL combs suppresses relative phase noise and linewidth broadening, ensuring that the RF beat notes retain the stability to accurately and reliably reproduce the optical spectral envelope, thereby enabling digital post-processing without loss of spectral fidelity. The processing pipeline consisted of the following steps: (i) Acquisition of RF signal and its power spectral density (PSD) estimation, (ii) Comb-line selection and interpolation, (iii) Inverted Gaussian fitting, (iv) Frequency-to-wavelength mapping, and (v) Calibration, validation and extraction of system performance metrics.

Firstly, transmission spectra were acquired using the custom built ADC-FFT module in single-shot measurements mode with a frame rate of ∼ 1.1 frames per second for each strain step. The resulting signal (PSD spectra) is the outcome of the down-converted OFCs passed through the FBG. These spectra provided the basis for calibration across different applied strain increments. Secondly, for each PSD trace, the resonance notch of the FBG was first identified by locating the initial dip (i.e., minimum amplitude) in the RF spectrum. Around this dip, a variable number of adjacent comb lines were selected to balance fitting stability against noise sensitivity. In practice, the selection of comb lines was guided by an initial reference spectrum acquired under pre-strained conditions for each FBG. This pre-strained DOFC-interrogated spectrum establishes the approximate spectral extent of the notch in the RF domain and, consequently, the number of comb lines overlapping the resonance. For each subsequent measurement, the algorithm identifies the initial dip and selects all comb lines spanning the local notch region, together with a small number of neighboring lines on either side (typically 2–4 additional tones per side) to stabilize the baseline estimation without introducing off-resonant noise. As a result, narrowband gratings like FBG2 (∼0.1 nm) are typically represented by 5–6 comb lines, whereas broader gratings such as FBG1 and FBG3 (∼0.3–0.5 nm) support a larger fitting window thus leading to denser sampling, as seen in Fig. 2 and Fig. 3.

To reconstruct a spectral profile suitable for curve fitting, linear interpolation was applied across the selected points. While the FBG spectral response can be rigorously modeled using coupled-mode/transfer-matrix methods [20], our objective here is not complete spectral reconstruction but robust estimation of the resonance shift from a limited number of comb samples. We therefore use an inverted-Gaussian surrogate to model the local notch region of the RF-domain envelope, as seen in Fig. 3a-d):

$$y(x) \; = \; a - b\exp\left(-\frac{(x-c)^2}{2d^2} \right) \tag{1}$$

where a is the local baseline, b is the notch amplitude, c is fitted parameter, corresponding to the effective Bragg frequency of the grating and d is the effective width, governing the curvature of the fitted notch. The model parameters were estimated using bounded nonlinear least-squares fitting implemented via the SciPy curve_fit routine. Initial parameter values were derived directly from step (i) by locally selecting comb samples under pre-strained conditions. To reduce sensitivity to initialization and prevent non-physical solutions, bounds were imposed during optimization, such as, $b > 0$, $d > 0$, $c \in [f_{min}, f_{max}]$, where f_{min} and f_{max} denote frequency limits of the selected fitting window, and a was constrained to within $\pm$ 10% of the estimated local maximum. Additionally, the power threshold value was also specified to avoid spectral floor noise. The final resonance frequency was obtained by evaluating the fitted model on a denser frequency grid via interpolation and selecting its minimum amplitude, further improving robustness under sparse spectral sampling.

This adaptive selection of comb lines ensures that the fitting procedure remains robust across gratings of different bandwidths, underpinning the bandwidth-independent applicability of the DOFC-IGF method, as seen in Fig. 3a-d). Additionally, this selection logic can be readily automated by monitoring the stability of fit metrics (e.g., R^2 or SSE) as the fitting window is tuned. The fitted notch-center frequency was then mapped back into the optical wavelength domain using the known RF–optical scaling determined by the DOFC repetition rates. This conversion ensures that the recovered values correspond directly to the physical Bragg-wavelength shifts of the FBGs, thereby linking the RF-domain IGF output to the true optical response of the sensor.

Calibration curves were obtained by plotting the extracted Bragg wavelength shifts against the applied strain values for different strain step sizes (strain increments) across both FBGs. Representative examples of these calibration plots are shown in Fig. 3e-f). The slopes of the calibration curves yielded the strain sensitivities (pm/με), while the standard deviation of the residuals provided the calibration error (σ_c). Additional performance metrics, including the standard deviation of residuals under pre-strained conditions over 300 s (σ_p), the coefficient of determination (R^2), and the sum of squared errors (SSE), were extracted
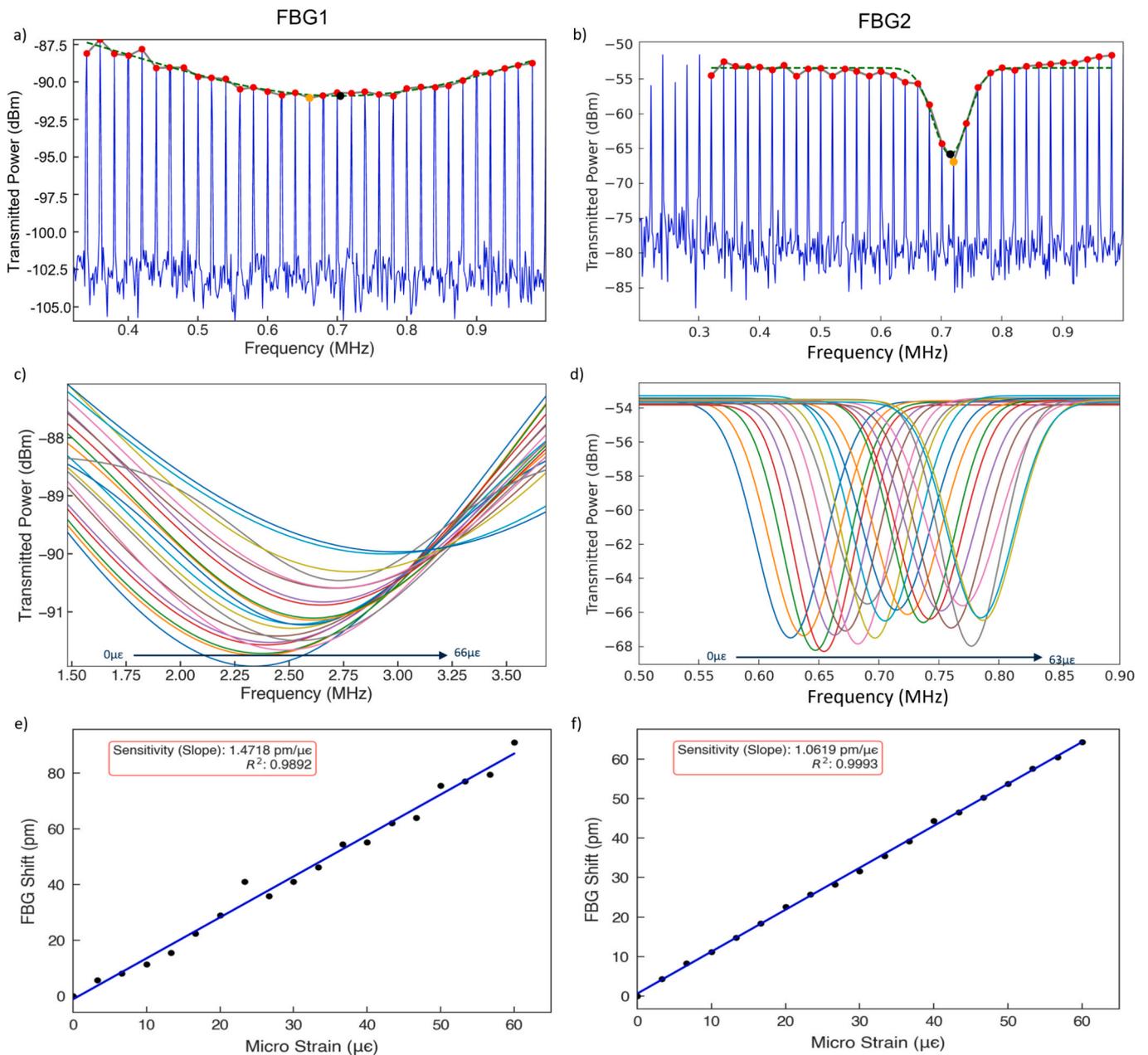
Fig. 3. Inverted-Gaussian fitting workflow for FBG1 (a, c, e) and FBG2 (b, d, f) with differing bandwidths − (a,b) representative fits, (c,d) aggregated fitted curves under increasing strain, and (e,f) corresponding strain-sensitivity results/ calibration plots, respectively.

to assess fitting fidelity and stability. From these quantities, the Figure of Merit (FoM) and effective strain resolution were subsequently determined as described in our previous work [4].

This methodology was applied uniformly to both FBG1 and FBG2, and their execution times for processing a single CSV file were found to be in the ranges of 340–350 ms and 152–170 ms, respectively. The sharper spectral dips of FBG2 (see Fig. 3d)), facilitated well-defined IGF despite its narrower bandwidth, while FBG1 exhibited broader but smoother features (see Fig. 3c)). In both cases, the processing pipeline enabled the consistent and repeatable extraction of Bragg wavelength even when 33 nε strain increments were applied, establishing the EI-GSL based DOFC interrogation scheme as a reliable high-resolution technique. On the other hand, the commercial Smart Scan interrogator data were processed using its internal algorithms and exported for direct comparison with the DOFC-derived calibration curves. By aligning strain steps, resolution, and sensitivity metrics, this approach enabled

rigorous benchmarking between the prototype DOFC platform and a widely adopted commercial standard, as discussed in the following section.

In the present implementation, the effective interrogation rate (~1.1 frames s^{-1}) is limited primarily by the prototype ADC-FFT module configuration and host-side data transfer, rather than IGF algorithm itself. The IGF fitting step operates on a small subset of comb lines and requires < 350 ms per frame in its current Python-based implementation. This processing time scales linearly with the number of tracked FBG notches and can be substantially reduced through compiled implementations or hardware acceleration. Importantly, neither the IGF algorithm nor the DOFC interrogation principle imposes a fundamental limitation on interrogation speed. Higher acquisition rates can be achieved by increasing the ADC sampling throughput, reducing averaging, or implementing the FFT and IGF steps on embedded hardware such as an FPGA. In addition, parallel fitting of multiple FBG notches enables

straightforward scaling to larger FBG arrays, with the primary practical constraints being available RF bandwidth, ADC dynamic range, and real-time processing resources rather than algorithmic complexity.

4. Results and discussion

The temporal stability of the DOFC interrogation was initially evaluated by analyzing the mean transmitted power and its 1σ fluctuation across the RF comb lines over 300 s, to verify that the measurements were not limited by short-term environmental perturbations. For FBG1 (see Fig. S2a), the fluctuation level was lower, ~0.18–0.28 dB, with a maximum of ~0.37 dB across 1–4 MHz, rising slightly where the mean-power envelope dips (~2.7–2.9 MHz). For FBG2 (see Fig. S2b), fluctuations are typically ~0.2–0.3 dB, with localized peaks up to ~0.55 dB (notably near ~0.2 MHz and ~0.9–1.2 MHz). These results indicate stable acquisition for both gratings, with FBG1 exhibiting better short-term stability under the present settings and confirming that the EI-GSL DOFC-FBG static strain interrogation system maintains per-line fluctuations at or below the 0.2–0.4 dB range over most of the band. Figs. S3 further corroborate the stability advantage of the DOFC-IGF pipeline. Time-domain wavelength fluctuations over 300 s reveal consistently lower noise floors for the DOFC (σ_p: 0.96 pm and 0.19 pm for FBG1 and FBG2, respectively, as seen in Fig. S3a-b), compared to the commercial interrogator (σ_p: 1.21 pm and 0.45 pm, respectively). This low noise level, along with an SNR of ~25–30 dB, underpins the high stability and repeatability of the subsequent strain calibrations. A longer-term stability measurement (60 h) is reported in [10], where an EI-GSL based DOFC exhibited maximum amplitude fluctuations of approximately 0.3 dB and a maximum wavelength fluctuation of less than 2 pm. With the optimization carried out on the DOFC operation, we anticipate that the results achieved here will be similar to the ones obtained in [10]. In future work, explicit temperature compensation will be implemented using a colocated strain-isolated reference FBG (or equivalent packaging) to separate strain and temperature contributions.

The calibration curves derived from the DOFC interrogation yielded sensitivities in the expected range for silica FBGs (~1–2 pm/με at 1550 nm), with linear responses sustained across strain steps from 3.33 με down to 33 nε. Fig. 4 and Fig. S4, report FBG1 calibration for strain steps of 3.33 με, 0.33 με, 0.17 με, and 33 nε, comparing DOFC-IGF (left column) with the Smart Scan interrogator (right column). The inverted-Gaussian analysis yields slopes of ~ 1.47, 1.63, 2.05, and 2.02 pm/με, clustered around the nominal silica-FBG value with consistently strong linearity (R^2 ~ 0.97–0.99). Whereas, the Smart Scan interrogator at corresponding με-level steps, demonstrated sensitivities of ~ 1.19, 1.20, and 0.97 pm/με, also with high linearity (R^2 ~ 0.98–0.99). However, at the finest 33 nε step, the fitted slope drops to ~0.50 pm/με and the goodness-of-fit degrades substantially (R^2 ~0.27), highlighting its inability to resolve minute FBG shifts. Repeated measurements under identical conditions confirmed this trend, with the response exhibiting poor repeatability and random variations rather than a consistent linear behavior. In contrast, the DOFC-IGF system consistently delivered linear behavior with the calibrated strains. Although both approaches provide
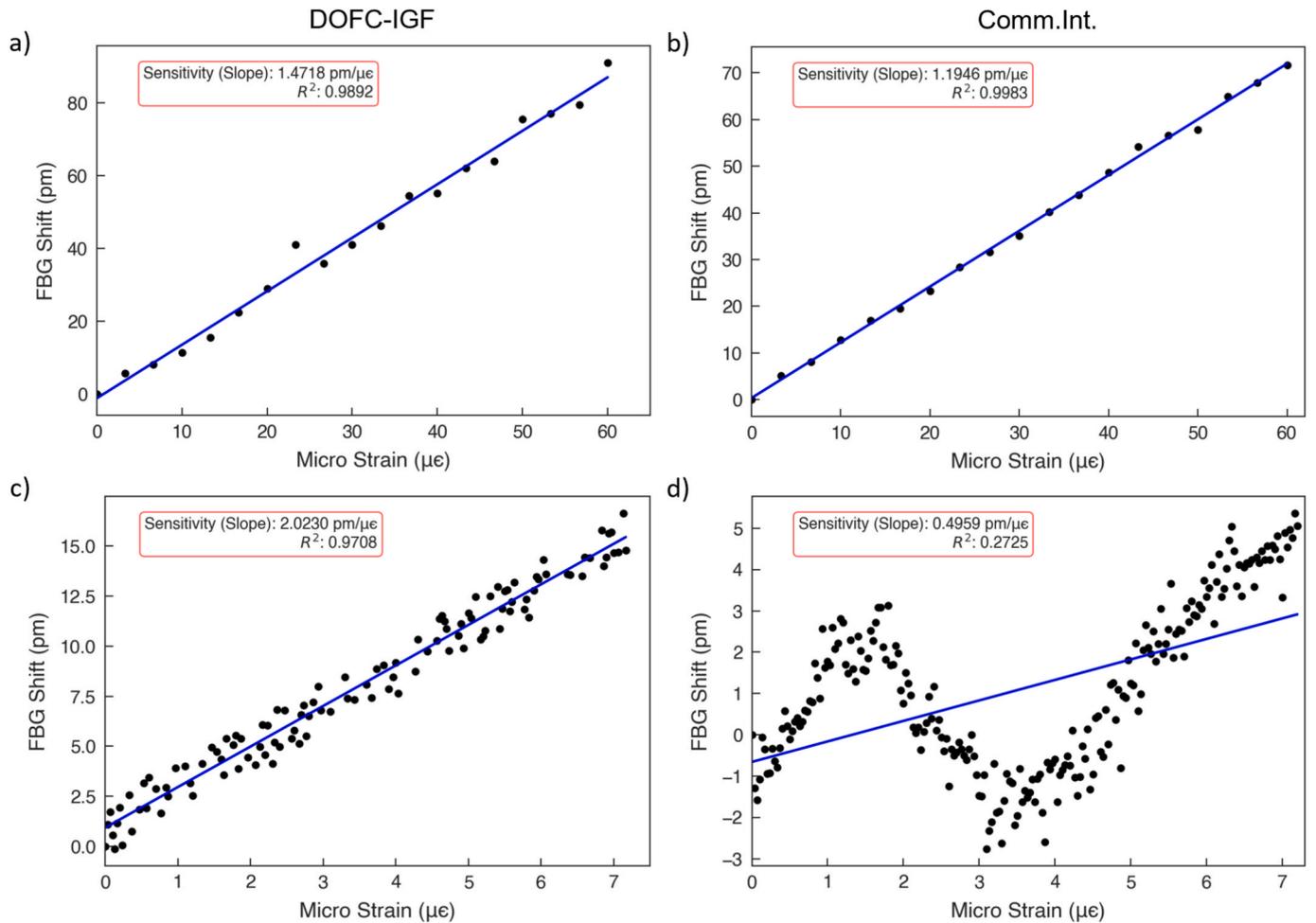

Fig. 4. Evolution of the FBG shift with the increment in the calibrated strain for the FBG1, when the applied strain increment is 3.33 με for a) and b); and 33.33 nε for c) and d). The plots in the left column correspond to data processed using the DOFC-IGF method, while the right column presents results from the commercial Smart Scan interrogator (Comm.Int.) operated at 2.5 Hz with 1000 averages and an effective integration time of 4.5 s.

monotonic, near-linear calibrations at the micro-strain level, the DOFC-IGF derived slopes remain stable down to the nano-strain level with higher sensitivities.

Similarly, Fig. 5 and Fig. S5, compare FBG2 calibration obtained from IGF (left column) and from the Smart Scan interrogator (right column) for strain steps of 3.33 με, 0.33 με, 0.17 με, and 33 nε. The inverted-Gaussian analysis yields sensitivities clustered near 1 pm/με (~ 0.94–1.07 pm/με) with excellent linearity (R^2 ~ 0.97–0.99). In contrast, Smart Scan regressions at the corresponding με-level steps report larger slopes (~ 1.52–1.96 pm/με) with slightly lower but still acceptable linearity (R^2 ~ 0.92–0.99). At the finest 33 nε step, the interrogator no longer resolves the Bragg shift reliably, following a similar trend to the interrogation of FBG1, where the fitted sensitivity falls to ~ 0.815 pm/με and the fit quality degrades drastically (R^2 ~ 0.53), pointing to a noise-dominated regime under these acquisition settings. The nanostrain-level calibration measurements were repeated multiple times under identical experimental conditions across 5 days, yielding consistent calibration slopes, residual distributions, and strain resolutions. Taken together, these results reaffirm that the DOFC-IGF pipeline maintains reliable, quantitative strain retrieval for both narrow and broadband gratings, whereas the commercial interrogator rapidly loses fidelity as the strain step approaches the nanostrain regime.

Analysis across gratings of different spectral widths confirms that, while the DOFC-IGF based interrogation exhibits some bandwidth dependence, its performance degrades far less with spectral width than that of commercial interrogators. Broad gratings (e.g., FBG2 and FBG3 with 0.5 nm bandwidth from [4]) yield more comb teeth across the notch, improving interpolation and producing better fits, while narrowband gratings (e.g., FBG2 at 0.1 nm) are sampled by only 5–6

comb lines under the tested configuration. Despite their intrinsically steeper slopes, this sparse sampling limits the resolution gains achievable with narrow FBGs and explains why FBG2 has a slightly lower resolution.

Table S1-S4 comprehensively compares the individual performances of FBG1 and FBG2 across various strain increments using both the DOFC-IGF pipeline and the commercial interrogator. Table 1 and Fig. 6 further summarize the comparative performance of the DOFC-IGF pipeline for FBG interrogation and the commercial interrogator across different FBG bandwidths and strain increments.

The FoM trends (see Fig. 6a) highlight that DOFC consistently achieves higher values, with FoM ~2.6 for 0.1 nm and ~2.1 for 0.3 nm gratings, and lower standard deviations (σ_c and σ_p) compared to the commercial system, underscoring its superior sensitivity and robustness at nanostrain scales. At microstrain levels, the DOFC-IGF pipeline outperforms the commercial interrogator for FBG1 up until 333.33 nε increments, whereas for FBG2, the DOFC-IGF pipeline clearly outperforms at the finest 33 nε steps and remains superior at 3.33 με increments. The cross-bandwidth analysis confirms that the DOFC maintains a reduced error ($\Sigma = \max(\sigma_c, \sigma_p)$) across narrow, mid, and broadband FBGs, particularly at the finest 33 nε increments (see Fig. 6b). Effective strain detection limit analysis, as shown in Fig. 6c, further confirms that the DOFC maintains sub-με performance across bandwidths of 0.1 nm, 0.3 nm and 0.5 nm, sustaining resolutions of ~380 nε, ~375 nε, and ~325 nε, respectively. In contrast, the commercial interrogator fails to resolve strain at the finest increments for both 0.1 nm and 0.3 nm gratings, and its performance deteriorates for the 0.5 nm FBG, where the resolution degrades to more than 478 nε. Linearity comparisons (see Fig. 6d) reveal similar trends, providing uniformly high coefficients of determination

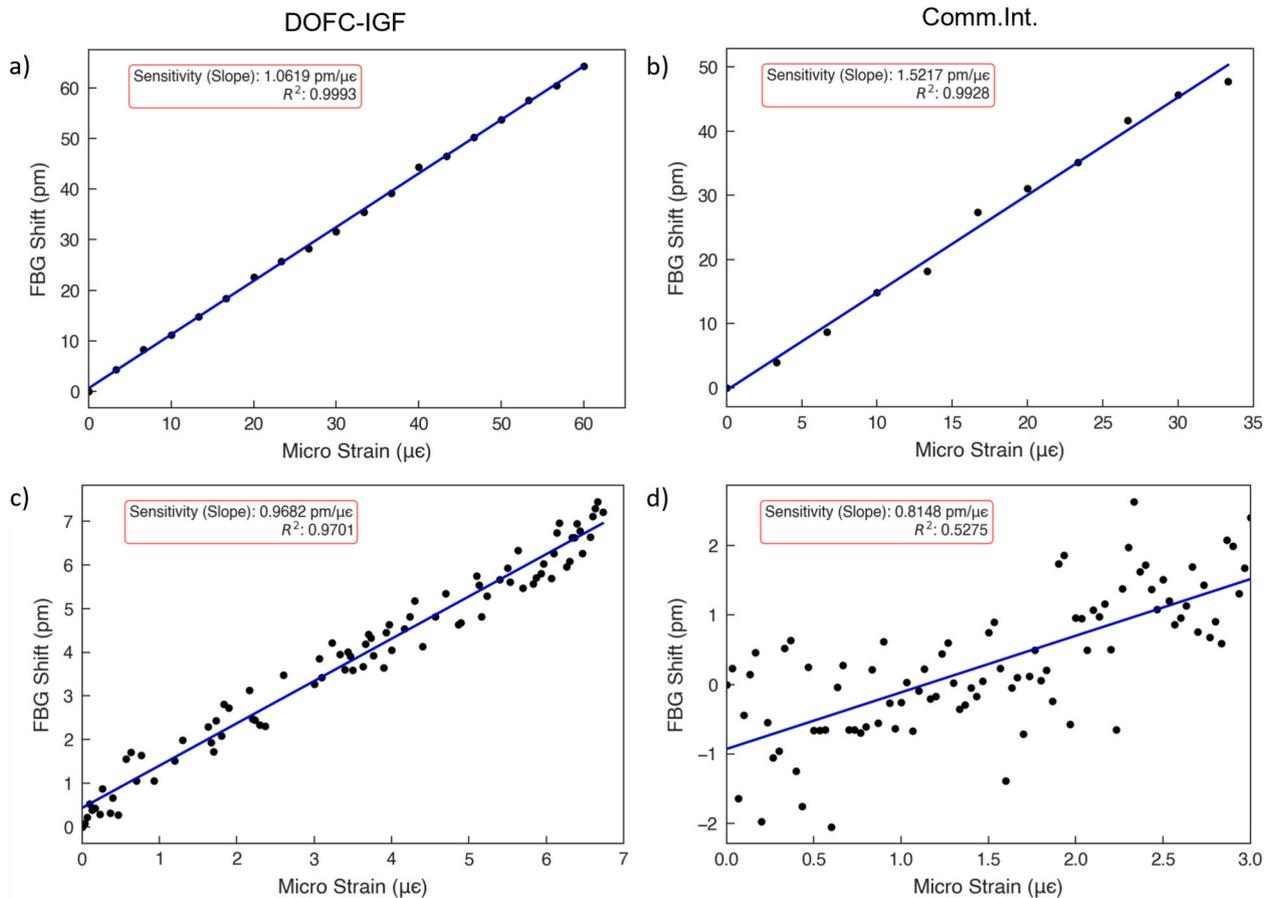**Fig. 5.** Evolution of the FBG shift with the increment in the calibrated strain for the FBG2, when the applied strain increment is 3.33 με for a) and b); and 33.33 nε for c) and d). The plots in the left column correspond to data analyzed using the DOFC-IGF method. The right column corresponds to data analyzed using the Smart Scan interrogator (Comm.Int.) with an acquisition rate of 2.5 Hz, 1000 averaging, and an integration time of 4.5 s.

Table 1
Performance summary for FBG1 (0.30 nm), FBG2 (0.10 nm), and FBG3 (0.50 nm) [4] under DOFC interrogation, with comparative entries for the commercial interrogator across bandwidths at 33nε increments.

| Bandwidth (nm)	Calibration error σ_c (pm)	Pre-strained error σ_p (pm)	Sensitivity S (pm/με)	Figure of Merit FoM	Effective strain detection limit EDL (nε)	Linearity R^2	Sum of squared errors SSE (pm^2)
DOFC-0.1	0.368	0.191	0.968	2.633	379.742	0.970	11.489
DOFC-0.3	0.758	0.958	2.023	2.112	374.724	0.971	64.938
DOFC-0.5	0.254	1.266	0.787	0.621	325.185	0.980	5.229
ComInt-0.1	0.679	0.434	0.815	–	–	0.528	41.481
ComInt-0.3	1.696	1.156	0.496	–	–	0.272	621.365
ComInt-0.5	0.564	1.341	1.179	0.879	478.128	0.819	32.758
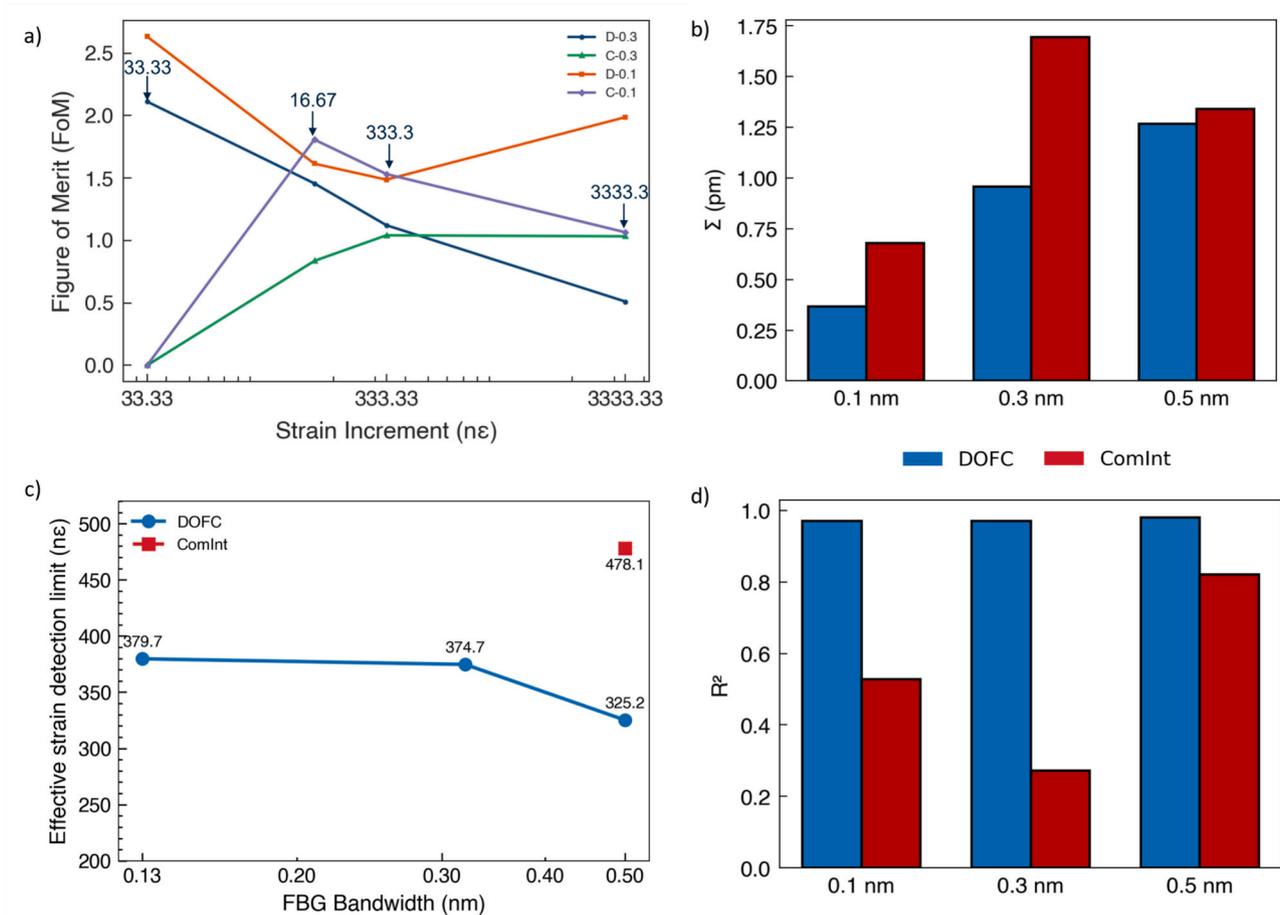
Fig. 6. a) Figure of merit (FoM) for FBG1 (D-0.3) and FBG2 (D-0.1) under DOFC-IGF interrogation compared with a commercial interrogator (C-0.3 and C-0.1) across varying strain increments, respectively. b) Comparison of maximum standard deviation ($\Sigma = \max(\sigma_c, \sigma_p)$) for FBG1 (0.30 nm), FBG2 (0.10 nm), and FBG3 (0.50 nm) under DOFC interrogation (in blue), with corresponding results from a commercial interrogator (in red) across bandwidths at 33 nε increments. c) Effective strain detection limit (EDL) and d) Linearity across different FBG bandwidths (0.1, 0.3, and 0.5 nm) interrogated using the DOFC system and a commercial swept-laser interrogator (ComInt).

($R^2 \sim 0.97$–0.99) for DOFC across all FBG bandwidths. However, the commercial system exhibits pronounced bandwidth dependence and poor regression quality for narrow (0.1 nm) and mid-range (0.3 nm) gratings.

Collectively, these results demonstrate that DOFC interrogation not only outperforms the commercial reference in sensitivity, linearity, and stability, but also delivers consistent performance across diverse FBG spectral regimes. This advantage primarily arises from the mutual coherence and optimized fitting, enabling DOFC interrogation to extend FBG sensing into the nano-strain regime, where commercial systems lose accuracy and reliability. Despite these advantages, the ultimate

performance of the DOFC-IGF pipeline remains intrinsically bandwidth-dependent. Narrower gratings may benefit more from denser comb sampling to improve dip reconstruction, while excessive densification in broadband gratings can introduce noise. In the current study, within this balance, the present system achieves a usable dynamic range of ~422 με for FBG1 and ~1300 με for FBG2, limited only by the DOFC spectral flatness characterized by 3 dB window of the individual combs.

5. Conclusions

We have demonstrated a dual optical frequency comb interrogation

system, based on externally-injection gain-switched lasers and coupled with an optimized inverted Gaussian fitting algorithm, capable of achieving sub-microstrain static strain resolution across fiber Bragg gratings of varying bandwidths. Unlike our earlier work, which focused on a single FBG bandwidth and various signal processing techniques to track FBG shifts, this study extends DOFC interrogation to a multi-bandwidth regime (0.1, 0.3, and 0.5 nm) and establishes, for the first time, a unified fitting strategy that remains robust under different spectral sampling conditions. Using a custom prototype ADC-FFT module, calibration tests with strain step sizes down to 33 nε confirmed that the DOFC-IGF pipeline sustains reliable wavelength-strain mapping, enabling sub-με resolution (~ 325–380 nε) while preserving robust linearity (R^2 ~ 0.97–0.99) and sensitivity in close agreement with reported literature values. In doing so, the system consistently outperformed a state-of-the-art commercial swept-laser interrogator across all tested spectral regimes. Comparative analysis revealed that although both DOFC and commercial systems exhibit certain bandwidth dependence, the mutual coherence of the combs and the adaptive IGF pipeline enable the DOFC platform to maintain superior sensitivity, lower calibration residuals, and significantly improved resolution.

These findings underscore the importance of balancing comb density with FBG bandwidth , while narrow gratings may benefit from denser comb sampling to stabilize fitting, excessive densification in broadband gratings risks amplifying noise. The demonstrated dynamic range of ~422 με and ~1300 με, combined with stable sub-με resolution and real-time compatible acquisition, positions the EI-GSL DOFC-IGF interrogation as a robust and scalable solution for high-precision strain sensing. More broadly, this approach provides a pathway toward compact, cost-effective sensor networks incorporating mixed-bandwidth FBG arrays, with applications ranging from structural health monitoring to precision metrology and next-generation photonic instrumentation.

CRediT authorship contribution statement

Malhar A. Nagar: Writing – original draft, Visualization, Validation, Methodology, Investigation, Formal analysis, Data curation, Conceptualization. **Minghao Wei:** Writing – review & editing, Validation, Resources, Methodology, Investigation, Data curation. **Alejandro Rosado:** Writing – review & editing, Software, Resources, Investigation, Formal analysis. **Conor McArdle:** Writing – review & editing, Software, Resources. **Aleksandra Kaszubowska-Anandarajah:** Writing – review & editing, Supervision, Resources. **Prince M. Anandarajah:** Writing – review & editing, Supervision, Resources, Project administration, Funding acquisition. **Davide Janner:** Writing – review & editing, Visualization, Supervision, Resources, Project administration, Investigation, Funding acquisition, Formal analysis, Conceptualization.

Declaration of competing interest

The authors declare that they have no known competing financial interests or personal relationships that could have appeared to influence the work reported in this paper.

Acknowledgements

Appendix A. Supplementary data

Supplementary data to this article can be found online at https://doi.org/10.1016/j.optlastec.2026.114840.

Data availability

10.5281/zenodo.17662199

References

[1] A. Rovera, A. Tancau, N. Boetti, M.D.L. Dalla Vedova, P. Maggiore, D. Janner, Fiber optic sensors for harsh and high radiation environments in aerospace applications, Sensors 23 (5) (Jan 2023) 2512, https://doi.org/10.3390/s23052512.
[2] M.A. Nagar, D. Janner, Polymer-based optical guided-wave biomedical sensing: from principles to applications, Photonics 11 (10) (Oct 2024) 10, https://doi.org/10.3390/photonics11100972.
[3] X. Li, Y. Li, S. Wu, Sub-100 fε resolution strain sensing based on an optical fiber frequency comb, Opt. Express, OE 33 (7) (Apr. 2025) 14655–14667, https://doi.org/10.1364/OE.551796.
[4] M.A. Nagar, M. Wei, C. McArdle, A. Kaszubowska-Anandarajah, P.M. Anandarajah, D. Janner, High-resolution FBG strain sensing with dual-comb interrogation and optimized signal processing, J. Lightwave Technol. 43 (15) (Aug. 2025) 7455–7466, https://doi.org/10.1109/JLT.2025.3567158.
[5] M. A. Nagar, 'Fiber Bragg Grating-Based Sensors: Advanced Techniques in Coating and Interrogation for Biomedical Applications', July 2025, Accessed: Sept. 29, 2025. [Online]. Available: https://iris.polito.it/handle/11583/3001930.
[6] M. M. M. Werneck, R. C. S. B. Allil, and F. V. B. de Nazaré, 'Interrogation Techniques of Fiber Bragg Gratings', in *Fiber Bragg Gratings: Theory, Fabrication, and Applications*, vol. TT114, SPIE, 2017, pp. 65–77. doi: 10.1117/3.2286558.ch6.
[7] I. Coddington, N. Newbury, W. Swann, Dual-comb spectroscopy, Optica, OPTICA 3 (4) (Apr. 2016) 414–426, https://doi.org/10.1364/OPTICA.3.000414.
[8] J. Guo, Y. Ding, X. Xiao, L. Kong, C. Yang, Multiplexed static FBG strain sensors by dual-comb spectroscopy with a free running fiber laser, Opt. Express, OE 26 (13) (June 2018) 16147–16154, https://doi.org/10.1364/OE.26.016147.
[9] P.M. Anandarajah, et al., Generation of coherent multicarrier signals by gain switching of discrete mode lasers, IEEE Photonics J. 3 (1) (Feb. 2011) 112–122, https://doi.org/10.1109/JPHOT.2011.2105861.
[10] E. P. Martin, S. T. Ahmad, S. Chandran, A. Rosado, A. A. Ruth, and P. M. Anandarajah, 'Stability Characterisation and Application of Mutually Injection Locked Gain Switched Optical Frequency Combs for Dual Comb Spectroscopy', *J. Lightwave Technol., JLT*, vol. 41, no. 13, pp. 4516–4521, July 2023.
[11] A. Kaszubowska-Anandarajah et al., 'Diverse sensing applications with dual optical frequency comb', in *Next-Generation Optical Communication: Components, Sub-Systems, and Systems XIV*, SPIE, Mar. 2025, pp. 27–30. doi: 10.1117/12.3038889.
[12] D.A. Poiana, J.E. Posada-Roman, J.A. Garcia-Souto, Compact interrogation system of fiber bragg grating sensors based on multiheterodyne dispersion interferometry for dynamic strain measurements, Sensors 22 (9) (Jan. 2022) 3561, https://doi.org/10.3390/s22093561.
[13] N. Kuse, A. Ozawa, Y. Kobayashi, Static FBG strain sensor with high resolution and large dynamic range by dual-comb spectroscopy, Opt. Express, OE 21 (9) (May 2013) 11141–11149, https://doi.org/10.1364/OE.21.011141.
[14] R. Zhang, Z. Zhu, G. Wu, Static pure strain sensing using dual–comb spectroscopy with FBG sensors, Opt. Express, OE 27 (23) (Nov. 2019) 34269–34283, https://doi.org/10.1364/OE.27.034269.
[15] M. Wei et al., 'Real-time FBG wavelength shift sensing system using a gain switched dual comb', in *2025 Optical Fiber Communications Conference and Exhibition (OFC)*, Mar. 2025, pp. 1–3. Accessed: Sept. 29, 2025. [Online]. Available: https://ieeexplore.ieee.org/document/11046627.
[16] T. Ideguchi, A. Poisson, G. Guelachvili, N. Picqué, T.W. Hänsch, Adaptive real-time dual-comb spectroscopy, Nat. Commun. 5 (1) (Feb. 2014) 3375, https://doi.org/10.1038/ncomms4375.
[17] T. Qing et al., *Dual-comb delay spectroscopy with attometer resolution*. 2020. doi: 10.48550/arXiv.2005.04673.
[18] X. Zhao, Q. Li, S. Yin, J. Chen, Z. Zheng, Dual-comb dynamic interrogation of fiber bragg grating with one mode-locked fiber laser, IEEE Sens. J. 18 (16) (Aug. 2018) 6621–6626, https://doi.org/10.1109/JSEN.2018.2852846.
[19] R. Zhou, S. Latkowski, J. O'Carroll, R. Phelan, L.P. Barry, P. Anandarajah, 40nm wavelength tunable gain-switched optical comb source, Opt. Express, OE 19 (26) (Dec. 2011) B415–B420, https://doi.org/10.1364/OE.19.00B415.
[20] S. Maiti, S. Prakash, V. Singh, Enhanced sensing performance of tapered profile in the apodized fiber Bragg grating for detection of cancerous cells utilizing their refractive index, J. Biophotonics 16 (12) (2023) e202300237, https://doi.org/10.1002/jbio.202300237.